JOURNAL OF PROPULSION AND POWER
Vol. 25, No. 3, May–June 2009

Thrust Measurement of the Hybrid Electric Thruster TIHTUS by a Baffle Plate

Hannah Böhrk*
DLR, German Aerospace Center, D-70569 Stuttgart, Germany
and
Monika Auweter–Kurtz†
Universität Hamburg, D-24129 Hamburg, Germany

DOI: 10.2514/1.34324

A novel, two-stage, electric thruster is under development at Institut für Raumfahrtsysteme at Universität Stuttgart. The first stage is an arcjet, and the second stage uses inductive heating of the arcjet plume. Because of the complex setup of the thruster, it is impossible to mount the two-stage system on a thrust stand without causing unwanted momentum onto the stand by the numerous supply lines. Thrust is, therefore, inferred using a baffle plate by means of a variation of power- and mass-flow ratios between the two stages. To interpret the results, the present paper also provides radially resolved measurement of total pressure from which thrust can be determined. It is shown that the thrust obtained from the two measurement methods are in good agreement with each other and range between 1.7 and 2.5 N for the respective operating conditions of the thruster. At constant total input power of 50 kW to the thruster, thrust decreases as power is diverted from the first stage to the second (inductive) stage at a constant mass-flow rate. However, when power is applied to both stages, thrust increases as the mass-flow rate is diverted to the second stage at a constant total mass-flow rate of 300 mg/s.

Nomenclature

A	=	area
c_e	=	effective exhaust velocity
d	=	plate diameter
DC	=	direct current (first stage)
e	=	thruster exit
el	=	electric
F	=	thrust
I	=	current
I	=	impulse
$L_{x,y,z}$	=	bearing force
m	=	mass
$\dot{m}$	=	mass-flow rate
Ma	=	Mach number
M_m	=	molecular mass
P	=	power
p	=	pressure
R	=	specific gas constant
RF	=	radio frequency (second stage)
S	=	sensor
stat	=	static
T	=	temperature
t	=	time
tot	=	total
η	=	efficiency
κ	=	isentropic coefficient
ρ	=	density
v	=	velocity
0	=	discharge chamber
∞	=	ambient
$*$	=	nozzle throat

Presented as Paper 5297 at the 43rd AIAA/ASME/SAE/ASEE Joint Propulsion Conference & Exhibit, Cincinnati, OH, 8 July 2007; received 10 September 2007; revision received 16 July 2008; accepted for publication 26 November 2008.

*Research Engineer, Institute of Structures and Design; hannah.boehrk@dlr.de.
†President. AIAA Fellow.

I. Introduction

THE current limitations to the exhaust velocity of hydrogen previously heated in a plenum of a rocket engine are imposed for various reasons. At low stagnation pressures, the bulk enthalpy added, although high, is largely transformed into dissociation and ionization but cannot be directed to kinetic energy when expanded to lower pressures in a nozzle. Or the bulk enthalpy is, although useful, low at high stagnation pressures. Or, finally, the enthalpy that can be converted to directed kinetic energy at optimum pressure shows a maximum but is a compromise between the two features mentioned previously. When both gas temperature and stagnation pressure are increased, the optimum will collide with limitations due to the electrode material [1]. Therefore, new thruster concepts are required in order to produce higher exhaust velocity at high thrust. High effective exhaust velocity c_e and high thrust F equate with thrust efficiency η_F to high input power P_{el} thrusters as in

$$P_F = \eta_F P_{el} = \frac{1}{2} F c_e \tag{1}$$

with

$$F = \dot{m} c_e \tag{2}$$

A promising concept is pursued with arcjet thrusters. They have been developed since the 1960s and provide relatively high thrust at moderate effective exhaust velocities [2,3]. Typical thrust ranges from 0.1 to 6 N for respective power input between 0.75 and 100 kW for a radiation-cooled design. Thrust efficiency, defined according to Eq. (1), is typically below 40% [4]. An arcjet thruster has a central cathode and an annular anode as sketched left in Fig. 1. The propellant is injected into the ring-shaped gap between the two electrodes and heated by an electric arc. It is then expanded and accelerated through a nozzle where the energy contained in the plasma is transformed to directed energy. These arcjet characteristics of high specific enthalpy are combined with the presence of a steep radial gradient as in a hot, energy-rich core with a relatively cold gas layer at its edge.

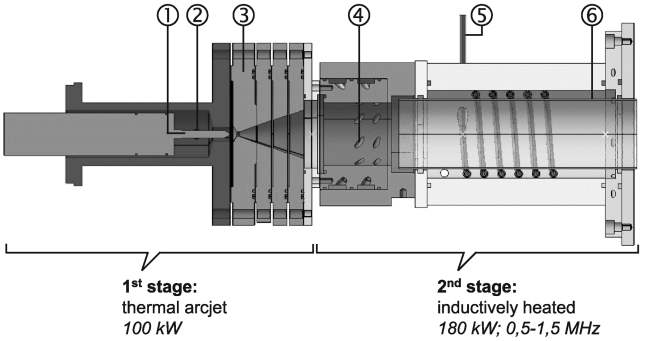

Fig. 1 Principle of TIHTUS, showing 1) cathode, 2) central gas supply, 3) anode, 4) swirl gas supply, 5) induction coil, and 6) discharge tube.

One approach to transfer more power into the plasma flow is to use an "afterburner" heating mechanism to reheat the edge of the plume without exceeding the material limitations mentioned previously. TIHTUS (Thermal-Inductive Hybrid Thruster of the Universität Stuttgart) is a two-stage plasma generator where reheating is realized by means of induction. The principle is sketched in Fig. 1. It has been developed Institut für Raumfahrtsysteme at Universität Stuttgart over the past four years [5–8]. This new concept has the potential to produce large thrust and high effective exhaust velocity by addition of power in the second stage [7]. It is, therefore, considered the predecessor of a future propulsion system for the transport of heavy payload on interplanetary trajectories [5].

Effective exhaust velocity c_e of any thermal thruster is dependent on the propellant temperature T_0 in the combustion chamber and the propellant molecular mass M_m according to

$$c_e \propto \sqrt{\frac{T_0}{M_m}} \tag{3}$$

The average propellant temperature should, therefore, be as high as possible. Currently, the highest effective exhaust velocities of thermal propulsion concepts that use stationarily chamber-heated hydrogen range between 20 and 25 km/s [2,4].

The flow from the arcjet stage of TIHTUS is supersonic in its center and subsonic at its edge. From an isentropic consideration of the conservation equations, it can be shown that heating of any supersonic flow has a decelerating effect on the flow [9]. It is, therefore, essential to find the coupling in which the power of the second stage does not yet couple into the supersonic core but raises the temperature of the cold gas layer and thereby increases the integral of the velocity of the flow.

The principle of superposed DC–RF plasma heating is not fundamentally new. Already in 1967 Vermeulen et al. [10] understood that one successful means of increasing specific thrust includes sequential heating of the plume of a DC arcjet. This was done by direct coupling of a high frequency (HF) electromagnetic field into the DC arcjet plume. A brief report on a hybrid plasma generator was given by Poole and Vogel [11] in 1971, and Yoshida et al. [12] presented a numerical characterization of DC–HF plasmas. Seo [13,14] reported on plume characterization of DC–HF hybrid plasma generators using enthalpy probes in the plume of a DC arcjet combined with a 25 kW inductive generator. Another DC–HF hybrid plasma generator is in operation at Tohoku University in Japan [15]. In all of the references mentioned here, hybrid plasma generators were applied within industrial applications such as thin film deposition, etc. As for the development of in-space propulsion systems, Leon and Mickelsen [16] present a basic theory of heat addition to supersonic flow of a resistojet by partial condensation of the vapor propellant.

A baffle plate, or impact target [17], is used for thrust monitoring of TIHTUS. It provides integral data of the plasma flow across the plasma plume. Furthermore, radially resolved Pitot pressure is given in order to interpret the results of the baffle plate experiment. Moreover, a method is presented to deduce thrust from it. Hence, thrust is determined from the calibrated baffle plate and compared with the thrust determined from integrated Pitot probe radial profile data.

After introducing the thruster principle, the present paper presents the setup of the ground test facility, the measurement principle and design of the baffle plate, and the setup of the Pitot probe. Furthermore, the methodology for determining thrust from Pitot pressure information is introduced. In the results section, the data are compared, and the latter method is evaluated according to the calibrated baffle plate data. It will be shown that with the present thruster design, pure arcjet flow still provides the highest thrust.

II. Thruster Concept

As mentioned previously, TIHTUS consists of an arcjet thruster (first stage) and an inductively heating afterburner (second stage). A view of the plasma thruster TIHTUS is shown in Fig. 2. The second stage consists of a discharge tube and a coil spun around it as part of a resonance circuit. The inductively heated plasma generator (IPG) is used as the afterburner because induction heating couples the power into the plasma at a radial position near the coil due to the skin effect [18]. In an arcjet plume, as mentioned in the introduction, this is the radial location of the cold gas layer. The plasma jet ejected from the arcjet is, thus, expanded into the quartz discharge tube. The alternating RF current in the coil induces an oscillating, mostly azimuthal, magnetic field inside the tube. This field initiates an electric discharge in the propellant oriented in the opposite direction of the coil current. The free electrons contained in the plasma from the thermal arcjet are accelerated by the electric field and, by means of collisions, transfer their induced power to the atoms and molecules. RF power is, thus, coupled into the plasma [19].

The thruster is operated as a water-cooled model using hydrogen as a propellant. However, at a further stage of development, the strategy foresees building the plasma source in a radiation-cooled design, promising an additional gain in exhaust velocity. Power may be coupled into the arc-heated (DC) or the inductively heated (RF) stage. Gas flow through the arc-heated stage is expanded first into the injection head of the inductive second stage where a swirl gas flow can be admixed. The principal question is whether it is possible to specifically heat the outer edges of an arcjet plume so that higher effective exhaust velocity can be attained. A dependency on the power staging between the two thruster stages is expected, as is a dependency on the gas mass-flow rate staging. Each operational condition is, therefore, referred to as T $P_{\mathrm{DC}}|P_{\mathrm{RF}} - \dot{m}_{\mathrm{DC}}|\dot{m}_{\mathrm{RF}}$ throughout this paper. As a result of the divergent gas jet being redirected through the straight discharge tube, the latter is strongly heated where the plume impinges on the quartz tube. At a power level of above 50 kW to the first (DC) stage at a mass flow of 300 mg/s, this can lead to melting and failure of the water-cooling seal [7]. Because of

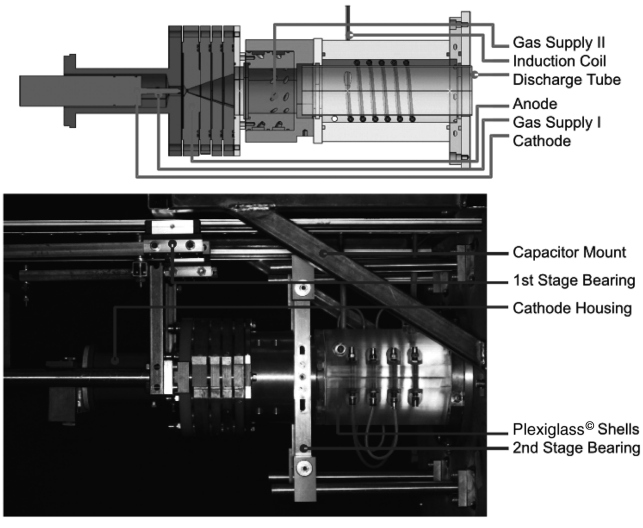

Fig. 2 Setup of TIHTUS.

Table 1 Nomenclature for operational condition

	P_{DC}, kW	P_{RF}, kW	$\dot{m}_{DC}$, mg/s	$\dot{m}_{swirl}$, mg/s
T 50|00–300|0	50	0	300	0
T 25|25–300|0	25	25	300	0
T 20|30–300|0	20	30	300	0
T 25|25–200|100	25	25	200	100
T 25|25–100|200	25	25	100	200

these tube-cooling limitations, although TIHTUS's first stage (the arcjet thruster) is capable of operation to up to 100 kW and its second stage is connected to a 180-kW radio-frequency power supply, the investigated operational conditions are limited to a sum of 50 kW of power input. The consequently investigated conditions are listed in Table 1.

Locally resolved measurements with probes show that for the condition of T 50|00–300|0, at axial distance of 200 mm from the thruster exit, the temperatures reach 6841 K at 9224 m/s velocity on the plume axis and approximately 2200 K at 4000 m/s at the plume edge [8]. Using electron properties from measurement in a comparable arcjet thruster [3], the mean free path of the electron-ion collision yields an order of 10^{-3} m. With these data, the collisional exchange time between the electrons and heavy particles is derived to be on the order of 10^{-7} s, whereas the residence time of the particles in the coil region is on the order of 10^{-5} s. This indicates that the thermal and chemical relaxation times are small compared with the convective timescale and heating of the gas passing through the second stage must, thus, be possible.

III. Experimental Apparatus

The TIHTUS ground test facility consists of the two plasma thruster stages and the vacuum chamber. A scheme of the facility is given in [5,7,8]. The size of the chamber is 3 m in length and 2 m in diameter. Installed are a gas supply system, water-cooling system, and a data acquisition system. The forward end cap of the vacuum chamber supports the thruster. The rear end of the chamber is connected to the vacuum pump system, the total volume flow rate of which is 6000 m^3/h at atmospheric pressure or 250,000 m^3/h at 10 Pa.

TIHTUS's first stage is a water-cooled arcjet thruster capable to be operated at up to 100 kW. It is operated by a 6 MW DC power supply. The second stage is connected to a 180-kW radio-frequency power supply with an external resonance circuit, which can be operated at frequencies ranging from 0.5 to 1.5 MHz. Both parts of the thruster are water-cooled at present. Therefore, thermal powers such as tube-cooling power loss or resonant circuit power are surveyed using resistance thermometers. They are electrically sealed and installed at an acceptable distance from the plasma source to prevent disturbing signals from the RF field. Additionally, the cooling water flow rates are measured. For gas dynamic plume investigation, a two-axis table is installed inside the vacuum tank on which probes can be mounted. Moreover, optical access is provided by viewports.

IV. Thrust Measurement

According to Newton, the propellant mass ejected from a thruster with thrust

$$F = \frac{\partial I}{\partial t} = \frac{\partial (mv)}{\partial t} \tag{4}$$

imposes an impulse on the thruster in the opposite direction. According to Eq. (4), two general approaches can be used for the experimental measurement of thrust. The first one is a direct measurement of the thrust exertion on the thruster, whereas the second approach is an indirect measurement of the impulse mv of the exhausted propellant (e.g., by means of a baffle plate or a Pitot probe).

Because of its unambiguousness and insensitivity to real effects such as the influence of assymmetry, the direct measurement method is mostly preferred [20]. However, it requires the thruster to be mounted on the thrust stand. In the present case, this means that the power supply of TIHTUS's DC stage, its RF induction coil, and cooling water lines have to be effected free of impulse. For the case of high DC power supply lines, the current is usually supplied via a mercury power feed. For the RF stage in which the discharge is effected by an induction coil, it must be taken into account that, due to the high Eigen frequency of the resonance circuit, the supply should have low inductance. Springs or mercury lines are, therefore, unacceptable. Hence, it is impossible to mount the two-stage system on a thrust stand without causing unwanted momentum transfer to the thrust stand by the numerous supply lines.

In the framework of the present research, two indirect measurement methods for thrust investigation of the two-stage hybrid electric thruster TIHTUS are used. These are thrust measurement by an impact target, the baffle plate, and by measurement and integration of a radial profile of total pressure.

The calibration of the baffle plate is performed by using the nominal thrust provided by the water-cooled thruster HIPARC-W. The thruster has a reproducible current-voltage characteristic and combustion chamber pressure dependent on mass-flow rate. The thrust F is repeatable for given operating conditions controlled by DC current I_{DC}, chamber pressure p_∞, and propellant mass-flow rate $\dot{m}$. It is assumed that the plasma plume from TIHTUS flows around the baffle plate similarly to the plume from the nominal thruster HIPARC-W.

HIPARC-W was investigated in a thrust stand of parallelogram type. The thrust stand used for calibration, the two methods of indirect thrust measurement, and their application for the present investigation are described next.

A. Parallelogram Thrust Stand

In the ground test facility the thruster is mounted in a beam construction [21,22]. The thrust from the device acts in the form of repulsion upon the beam construction. To measure the thrust, the construction is arranged on knife-edge bearings on a cantilever. The parallelogram form of the thrust stand is used so that only horizontal deflection is measured, see Fig. 3.

Effective exhaust velocity of HIPARC-W, defined as

$$c_e = F/\dot{m} \tag{5}$$

and thrust are shown in Figs. 4 and 5. The thrust stand is calibrated under a vacuum by means of weights just before each measurement run. The force sensor is of double-cantilever type with strain gauges. The error determined by the calibration investigations is ±0.1 N.

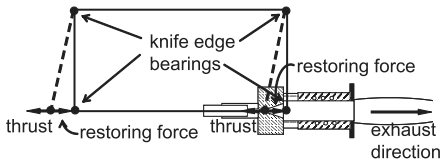

Fig. 3 Restoring force.

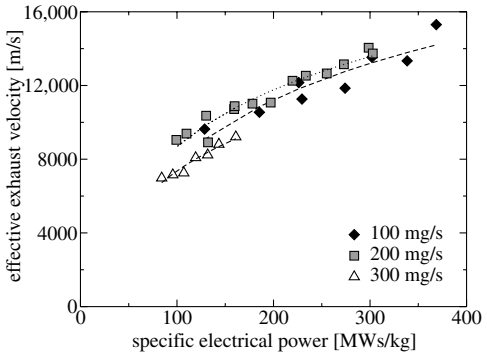

Fig. 4 Effective exhaust velocity of HIPARC-W.

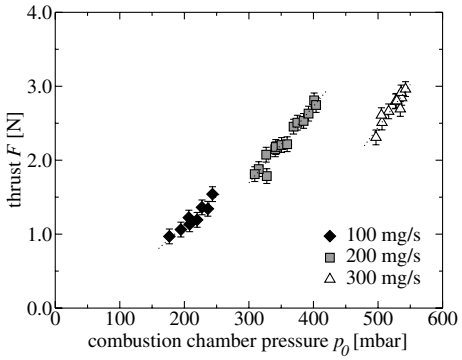

Fig. 5 Thrust of HIPARC-W.

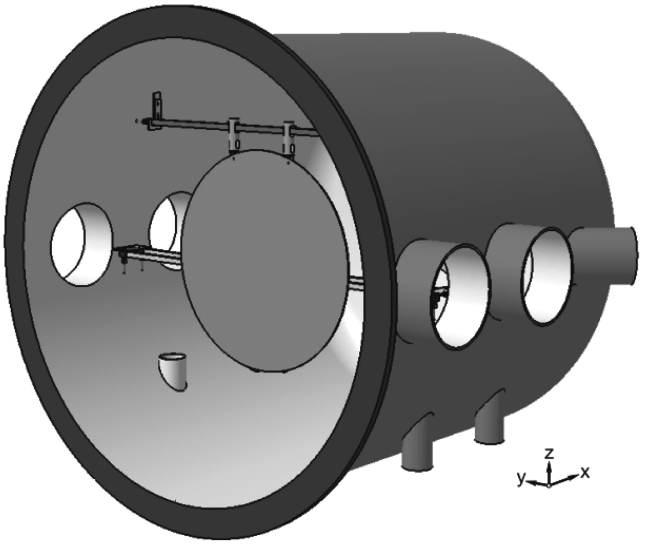

Fig. 6 Baffle plate in the vacuum chamber.

The baffle plate is calibrated using the thrust from the nominal thruster HIPARC-W, which was investigated by means of the parallelogram thrust stand. The scaling is based on the assumption that thrust from the HIPARC-W is repeatable for the same operating conditions.

B. Baffle Plate

To provide a device for thrust measurement in complex thruster systems, a so-called baffle plate, also referred to as impact target, was developed in the framework of the present research. Thus, with this device the rather complex two-stage thruster does not need to be mounted on a thrust stand.

With the plasma generator attached to the forward end cap of the tank (not in the sketch of Fig. 6), the baffle plate is suspended on knife edges and hung across the plasma column as depicted in Fig. 6. Its center is aligned with the plume axis so that a symmetric flow is assumed. The aerodynamic effects such as lift or drag of the impact plate are minimized when the angle of deflection is zero. With the deflection being acted against by a force transducer based on a restoring force, the thrust can be determined without any

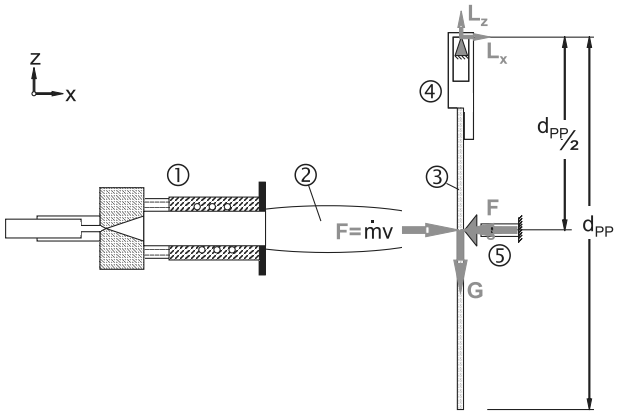

Fig. 7 Measurement principle of the baffle plate showing 1) thruster, 2) plasma plume, 3) baffle plate, 4) bearing, and 5) force transducer.

aerodynamic influences. The sensor is a typical strain gauge Wheatstone bridge configuration so that temperature dependency is minimized. According to Fig. 7, for momentum equilibrium the following equations can be noted according to

$$L_x + F_S - F = 0 \tag{6}$$

$$L_y - G = 0 \tag{7}$$

and

$$F\frac{d}{2} - F_S\frac{d}{2} = 0 \tag{8}$$

It can be seen from Eqs. (6) and (8) that the momentum in flow direction x is zero and the thrust F can, therefore, be measured directly.

The plate is a 5 mm-thick copper plate with a diameter of 1 m. This is much larger than the plasma plume proportion of <200 mm. The plate weighs about 50 kg. It was especially developed for thrust measurement of TIHTUS. The thruster is operated continuously, and both the arcjet and the inductively heated stage are high-enthalpy and high-power plasma sources. The heat load onto the baffle plate is, therefore, the critical factor for the measurement. The plate consists of copper, which has high thermal heat capacity. The high temperature can, thus, be conducted away from the center. Uncooled, however, it warps under inhomogeneous heat load and the measurement becomes erratic. Therefore, the baffle plate carries a water-cooling spiral on its rear side, as shown in Fig. 8. For the water not to apply a momentum onto the plate, supply lines are directed into opposed directions and perpendicular to the thrust vector (i.e., in L_y-direction).

The mean deviation of the measured data from the nominal thrust data was determined to ± 0.17 N, including the uncertainty of the strain gauge used in the baffle plate setup of ± 0.05 N. The calibration data and regression curves are displayed in Fig. 9, where the data is sorted according to mass-flow rate. Including the thrust stand's error of 0.1 N, the mean measurement certainty results in ± 0.27 N. The regression curve chosen is based in the assumption that with TIHTUS the flow generated around the baffle plate is similar to that of the nominal thruster HIPARC-W. Given this

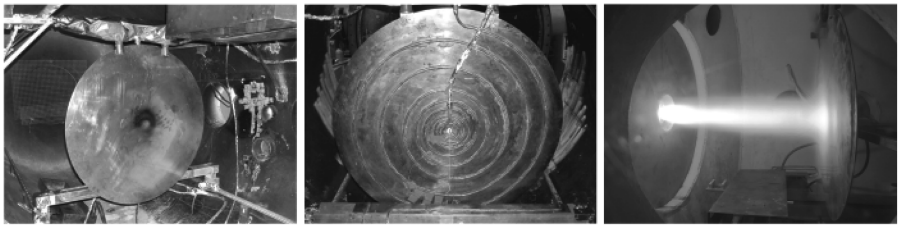

Fig. 8 Front and aft side of the baffle plate and during an experiment.

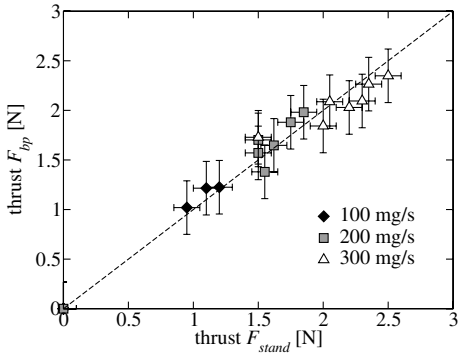

Fig. 9 Thrust calibration.

assumption, this method calibrates out any momentum reflection of the propellent onto the baffle plate, boundary influence in the flow around the baffle plate, the entrainment of rest gas from the vicinity, as well as temperature effects, so that these do not explicitly need to be taken into account. The control and measurement of the current and voltage have a deviation of up to 0.5% from the true value, so that the electric power deviates as little as 1%. Mass-flow measurement also deviates only 1% from the true value so that in consequence the deviation of the operation condition from the aspired condition is negligible in comparison to the uncertainty of the baffle plate measurement.

C. Determination of Thrust from Pitot Pressure

The total or Pitot pressure is the pressure present in the foremost stagnation point of a body inserted into a plasma column, such as a Pitot probe. Assuming that within the probe the deceleration of the flow takes place isentropically, which is reasonable because the heat transfer within the probe cavity is small for hydrogen, the pressure measured at the end of a Pitot tube corresponds to the total pressure in the stagnation point in front of the tube opening. At $Ma \geq 1$, this is the plenum pressure just behind an imaginary, vertical, ideal bow shock. In a supersonic flow, the Pitot probe, therefore, does not measure the total pressure in the free stream. The ratio of the true total pressure of the free stream to the measured total pressure behind a bow shock is [23]

$$\frac{p_{\mathrm{tot},1}}{p_{\mathrm{tot},2}} = \left(\frac{2\kappa}{\kappa+1}Ma_1^2 - \frac{\kappa-1}{\kappa+1}\right)^{\frac{1}{\kappa-1}} \left(\frac{1+\frac{\kappa-1}{2}Ma_1^2}{\frac{\kappa+1}{2}Ma_1^2}\right)^{\frac{\kappa}{\kappa-1}} \tag{9}$$

The Pitot probe used in the present case is of European standard geometry (flat nose, 50 mm body diameter, rounded edge) with a measurement orifice of 26 mm in diameter. It is depicted in Fig. 10. In the present work, the plume of the two-stage thruster TIHTUS is investigated by this Pitot pressure probe. For proof of repeatability, each measurement point was detected twice, and mean values are presented here. In the following, a method is introduced in which the thrust can be determined from the radial profile of the total pressure.

Fig. 10 Pitot probe.

Mach number is defined as

$$Ma = \frac{v}{a} = \frac{v}{\sqrt{\kappa RT}} \tag{10}$$

Depending on Mach number, in the stagnation point a total pressure is formed so that

$$\frac{p_{\mathrm{tot}}}{p_{\mathrm{stat}}} = \left(\frac{2\kappa}{\kappa+1}Ma^2 - \frac{\kappa-1}{\kappa+1}\right)^{\frac{1}{1-\kappa}} \left(\frac{\kappa+1}{2}Ma^2\right)^{\frac{\kappa}{\kappa-1}} \tag{11}$$

in supersonic and

$$\frac{p_{\mathrm{tot}}}{p_{\mathrm{stat}}} = \left(1 + \frac{\kappa-1}{2}Ma^2\right)^{\frac{\kappa}{\kappa-1}} \tag{12}$$

in subsonic flow [9]. Both isentropic exponent κ and specific gas constant R are functions of temperature. It was shown by Laure [24] that a deviation of the isentropic exponent has only little influence on the result of Mach number derived from Eq. (11). The data presented here are, furthermore, based on the assumption that the ambient pressure in the vacuum tank p_∞ is imposed on the plasma plume so that $p_{\mathrm{stat}} = p_\infty$. This assumption is also supported by Laure et al. [25] and Abramovich [26].

Total pressure measurements can also be used to determine the thrust of a device [27]. Under use of mean values, thrust can be determined according to

$$F = \dot{m}\,\bar{v} + (\bar{p}_e - p_\infty)A_e = \dot{m}c_e \tag{13}$$

The control volume for the consideration of Eq. (13) was laid around the thruster and ended at the exhaust plane of the thruster. The pressure p_e is the static pressure at the exhaust plane A_e of the control volume (i.e., the thruster). It is depicted in Fig. 11. Figure 12 shows a control volume ending 200 mm downstream of the thruster. The consideration of Eq. (13) extended to this control volume, where $p_e = p_\infty$, results in

$$F = \dot{m}\,\bar{v} \tag{14}$$

With the mass conservation equation

$$\dot{m} = \rho v A \tag{15}$$

and the state equation for a perfect gas [9,28,29]

$$p = \rho RT \tag{16}$$

$\dot{m}v$ becomes equal to $\frac{p}{RT}v^2A$ and extended with the isentropic exponent Eq. (13) yields

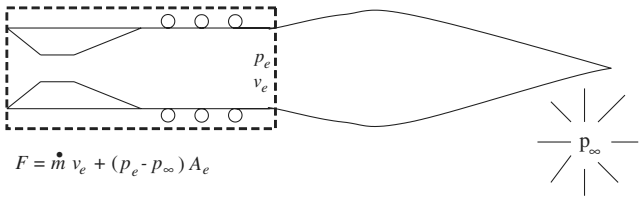

Fig. 11 Control volume across thruster exit plane.

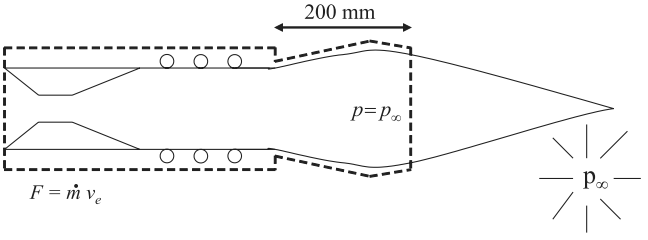

Fig. 12 Control volume across plume cross section at $x = 200$ mm.

$$F = \int_A \frac{\kappa p}{\kappa RT} v^2 \mathrm{d}A = \int_A p\kappa Ma^2 \mathrm{d}A \tag{17}$$

The plasma plume is assumed to be rotationally symmetric. No energy dissipation is regarded by vortices at the plume edge, and no mass entering from the vicinity into the plume is considered. Fasoulas et al. [30] found out that an admix of ambient air into the plasma plume actually takes place. However, this effect is neglected in the current interpretation. The thrust determination is, thus, only dependent on the Mach number and isentropic coefficient, whereas the Mach number is only dependent on the ambient and total pressure.

In the experiment, the data points are integrated across the plume cross section by summation according to

$$F = \sum_i F_i = p_\infty \sum_i \kappa_i Ma_i^2 A_i \tag{18}$$

where A_i is the ring segment of the respective position i in the rotational symmetric plasma column and determined as $r_{i+1}^2\pi - r_i^2\pi$. It was shown by Hiers and Pruitt [27] that determining the thrust from Pitot pressure is not very sensitive to the Mach number or the isentropic exponent.

V. Results and Interpretation

As was described in the introduction, in TIHTUS, electric power can be applied to either the arc-heated stage, the inductively heated stage, or to both stages. Also, the ratio of the gas flows through either stage can be varied. The five operating conditions of Table 1 were investigated. They include a variation of power staging for a gas flow relation of 300|0 mg/s and a variation of mass-flow staging for constant power staging of 25|25 kW.

Thrust is measured with the baffle plate and radial profiles of total pressure are measured by means of the Pitot probe. Radial profiles were investigated at an axial position of $x = 200$ mm, and the baffle plate is located at $x = 860$ mm from the thruster exit.

A. Thrust and Thrust Efficiency

The thruster was first investigated under cold gas operation. The pressure p_0 in the combustion chamber for a gas supply of 300|0 mg/s was measured to be 209 hPa. With the analytical approach for a matched nozzle, providing ambient pressure at the nozzle end, the cold gas thrust is estimated as

$$F = p_0 A^* \left(\sqrt{\kappa \left(\frac{2}{\kappa+1}\right)^{\frac{\kappa+1}{\kappa-1}}} \sqrt{\frac{2\kappa}{\kappa-1}} \sqrt{1 - \left(\frac{p}{p_0}\right)^{\frac{\kappa-1}{\kappa}}} + \frac{A_e}{A^*} \left(\frac{p_e - p_\infty}{p_0} \right) \right) = 1.04 \text{ N} \tag{19}$$

with the nozzle cross section A^*, the thruster exit area A_e and $\kappa(T) = 1.4$. The thrust measured at this mass-flow rate was 0.98 N, showing that the measurement data are reliable. The thrust measured with the baffle plate at cold gas conditions (i.e., no power input) are depicted in Fig. 13. The full circles are measurement points of thrust at the respective mass-flow rates without any electric power supplied. Small circles show the standard deviation of the mean thrust values according to $\Delta\bar{F} = \sqrt{\sum_{i=1}^{n}((F_i - \bar{F})^2/n(n-1)}$. Each condition was rerun approximately four times. It is found that at an overall mass flow of 300 mg/s, the larger the mass-flow fraction supplied by the RF stage, the smaller the thrust. This results because the flow $\dot{m}_{\mathrm{RF}}$ is admixed downstream of the nozzle and is, therefore, not explicitly accelerated. Moreover, the gas is injected tangentially instead of axially and, therefore, has a smaller impulse due to smaller axial velocity.

Figure 14 shows TIHTUS thrust at a mass-flow rate of 300|0 mg/s. The circles, again, denote the measurement values. The area depicted in between these points is an interpolation in order to indicate a trend of the thruster behavior. The thrust is largest with 2.04 N for the operating condition T 50|00–300|0, which is a pure arcjet condition. For decreasing power supplied to the first (arcjet) stage, thrust also decreases. With the same mass-flow staging but with power staging of 25|25 kW, the measured thrust is lower with 1.85 N. At 20|30 kW, the thrust measured is even smaller with 1.66 N. The power is obviously not transferred to thrust and effective exhaust velocity effectively when the second stage is in operation. A possible explanation lies in the fact that the power may couple into the supersonic plume core. Heating of a supersonic flow is known to decelerate the flow velocity [9]. Moreover, the inductive portion of the power added in the second, geometrically cylindrical part of the thruster cannot be effectively accelerated. However, it can be seen from Fig. 14 that at constant DC power the thrust increases for increasing RF power. It is, therefore, likely that a large portion of the power can be recovered by a design optimization.

In Fig. 15, thrust power of the two-stage hybrid thruster is shown. According to Eq. (1), thrust efficiency was also derived for these measurement points. And it turns out that although second-stage operation causes a thrust increase, thrust efficiency decreases while second-stage power is increased.

Gas flow rate staging was also investigated. Its results are presented in Fig. 16, where operating points always add up to a sum of 300 mg/s. 200|100 is indicated where $\dot{m}_{\mathrm{RF}}/(\dot{m}_{\mathrm{DC}} + \dot{m}_{\mathrm{RF}})$ equals 0.6. The power staging was kept constant. Generally, it can be noted that the mass-flow staging does not have great influence on the thrust. However, when the second stage is inactive but mass flow to the second stage is increased, thrust decreases. As mentioned previously, the mass flow to the second stage is injected tangentially so that no axial impulse is imposed on the flow. It is, therefore, plausible that axial injection with additional acceleration in a converging–diverging nozzle results in higher impulse of the flow. Nonetheless,

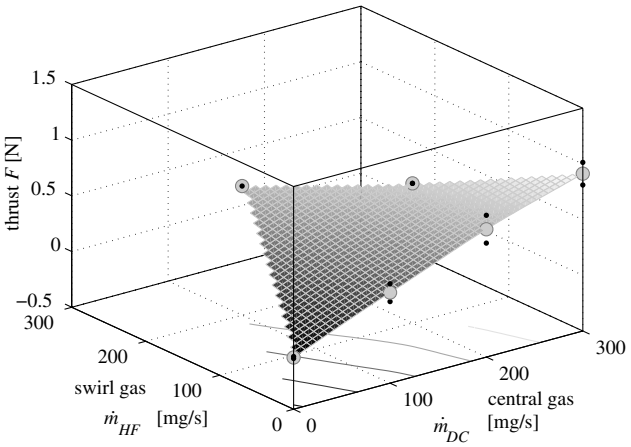

Fig. 13 Cold gas thrust at variable mass-flow rates.

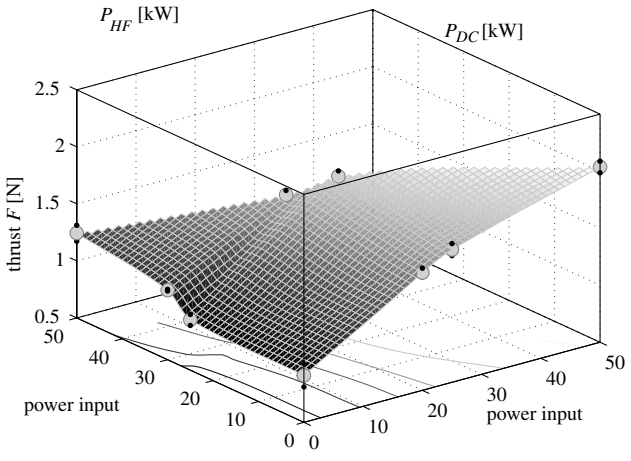

Fig. 14 Thrust at a mass-flow rate of 300|0 mg/s.

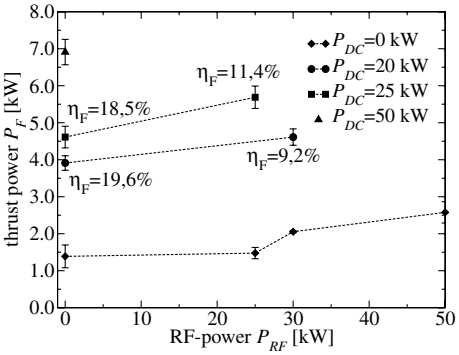

Fig. 15 TIHTUS's thrust power vs second-stage (RF) power at various DC power.

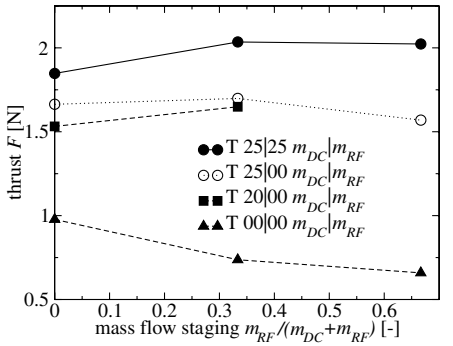

Fig. 16 Thrust at various power staging over gas flow staging.

with the second stage active, it seems that a tendency of increasing thrust can be spotted from the curve with full circles in Fig. 16. Constant power of 25 kW is supplied to the arcjet stage while the mass-flow rate is reduced. The specific power in the arcjet plume is, therefore, increased. In this comparably energy-rich plasma, the tangentially supplied mass flow is admixed. At an increasing second-stage mass-flow rate, the cold mass flow mixes in better with the hot plasma from the arcjet, resulting in higher plasma electrical conductivity in the coil region, leading to better coupling to the plume.

B. Pitot Pressure

Figure 17 shows Pitot pressure in the plane perpendicular to the plume exhaust direction and 200 mm downstream from the nozzle exit with a mass-flow rate of 300 mg/s through the arcjet thruster stage. The maxima at excentric position is typical for high mass-flow rates and corresponds to the behavior known from the literature [24]. A key influence is given by the nozzle, the radial distribution of mass-flow rate, and the plasma flowing through the discharge tube instead of a diverging nozzle. The curve marked with hollow triangles represents only the arc-heated stage active at 20 kW. It shows maxima at the excentric position, although the plume is quite narrow. Black triangles mark the same arcjet power with second-stage power added to it. It becomes evident that the power of the inductively heated stage is coupled into the plasma annularly at the excentric position.

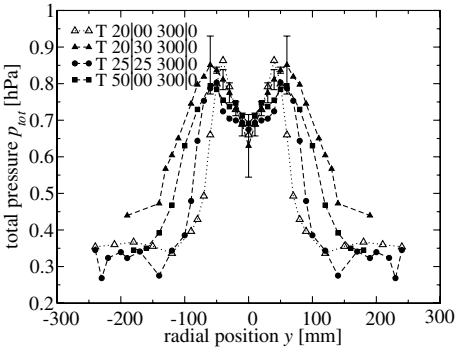

Fig. 17 Variation of Pitot pressure with power partitioning.

The black symbols represent conditions with power staging adding up to 50 kW each. At the plume center, it can be observed that higher total pressure is produced with increasing arc power at constant total power. The highest excentric maxima representing a total pressure of 0.85 hPa are achieved with 20 kW supplied from the arc heating stage and 30 kW, that is T 20|30–300|0, coupled into the plume by inductive heating. The same condition results in the widest plume diameter although the Pitot pressure is lowest at the plume axis. This can be interpreted as the most power coupled into the plasma at the near-coil position. However, the smallest diameter is *not* reached at pure arc heating with 50 kW but with 25 kW arc and 25 kW inductive heating. The error bars displayed in Fig. 17, contain the inaccuracy of the pressure transducer and the standard deviation of the measurement points. Each point was investigated approximately three times.

For maintained power staging of 25|25 kW, a gas flow variation was conducted. The respective Pitot pressure graphs are presented in Fig. 18. From the edges of the plume, it can be seen that according to the measurement condition and the mass-flow staging, the ambient pressure in the tank varies between 0.34 and 0.4 hPa. At radial positions >130 mm, a turbulent outer region of the plume can be noticed. This may also indicate an admix of ambient air into the plume edge. In the second stage, the gas flow is injected radially as swirl gas. It has been observed that the more gas injected as swirl gas, the higher the ambient pressure or the admix of ambient air. The diameter of the plasma plume, however, does not remarkably change with varying mass-flow staging. Total pressure maxima of 0.85 hPa are reached for 100|200 mg/s.

VI. Conclusions

Thrust was measured in the two-stage, hybrid, electric thruster TIHTUS by means of a baffle plate. The baffle plate was calibrated using the nominal thrust provided by the arcjet thruster HIPARC-W. A second thrust measurement was performed by a Pitot probe. With

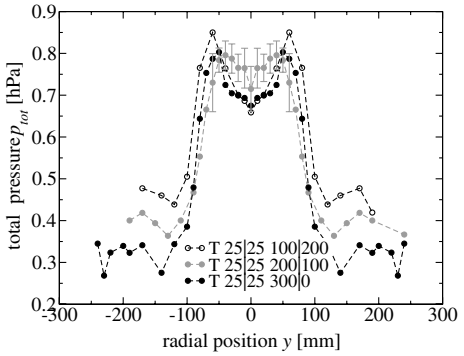

Fig. 18 Variation of Pitot pressure with mass-flow rate partitioning.

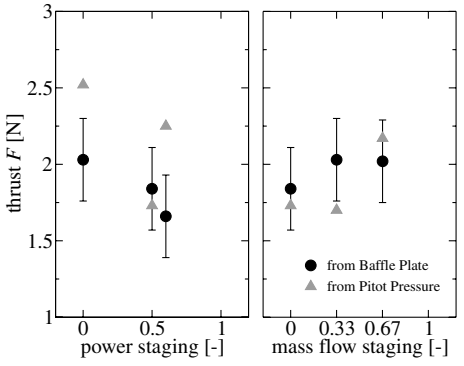

Fig. 19 Results of thrust measurement for power staging $\frac{P_{RF}}{P_{DC}+P_{RF}}$ at fixed mass-flow rate of 300|0 (left) and mass-flow staging $\frac{m_{RF}}{m_{DC}+m_{RF}}$ at a fixed power ratio of 25|25 (right).

the method described previously, thrust was determined from the Mach number deduced from the Pitot probe measurement. The range of Mach numbers encountered yields values between 1.2 and 1.4 at the radial maxima. The determined thrust data are compared in Fig. 19. Two major influences on the thrust values were isolated during the evaluation of the experiments. These are ambient pressure and integration depth (i.e., the radius over which thrust is integrated). The rest of the data are in good agreement with each other with a deviation below 25%. However, in order to verify that the determination of thrust from Pitot pressure is admissible, Pitot pressure ought to be measured and integrated at various axial positions.

It can be seen that for decreasing first-stage power and increasing power to the second (inductive) stage, the flow of which is not expanded through a nozzle, thrust decreases. At constant power partitioning and constant sum of mass-flow rates, an increasing mass-flow rate injected downstream of the nozzle in the second stage increases the thrust.

Acknowledgments

The authors wish to thank their students Robert Schieb, Melanie Lücke, and Markus Mayer for their contributions to the experiments presented here. Their colleague Uwe Bauder kindly presented the results at the 43rd AIAA/ASME/SAE/ASEE Joint Propulsion Conference and Exhibit, in Cincinnati, Ohio.

References

[1] Bonneville, J. M., "High-Frequency Supersonic Heating of Hydrogen for Propulsion," *AIAA Electric Propulsion Conference*, AIAA 1963-26, March 1963.

[2] Wallner, L. E., and Czika, J., "Arc-Jet Thrustor for Space Propulsion," NASA TN-D-2868, 1965.

[3] Auweter–Kurtz, M., Gölz, T., Habiger, H., Hammer, F., Kurtz, H., Riehle, M., and Sleziona, C., "High-Power Hydrogen Arcjet Thrusters," *Journal of Propulsion and Power*, Vol. 14, No. 5, 1998, pp. 764–773. doi:10.2514/2.5339

[4] Auweter–Kurtz, M., "*Lichtbogenantriebe für Weltraumaufgaben*," B.G. Teubner, Stuttgart, Germany, 1992.

[5] Böhrk, H., Schmidt, T., and Auweter–Kurtz, M., "Flexible Piloted Mars Missions Using the TIHTUS Engine," *Aerospace Science and Technology*, Vol. 11, Nos. 2–3, 2007, pp. 211–221. doi:10.1016/j.ast.2006.10.002

[6] Böhrk, H., and Auweter–Kurtz, M., "Efficiency Analysis of a Two-Stage Hybrid Electric Thruster," *Journal of Thermophysics and Heat Transfer*, Vol. 22, No. 2, 2008, pp.309–312.

[7] Böhrk, H., and Auweter–Kurtz, M., "Preliminary Results of TIHTUS Operation," AIAA Paper 2006-5158, July 2006.

[8] Böhrk, H., and Auweter–Kurtz, M., "Velocity and Total Pressure Measurement in the Two-Stage Hybrid Thruster TIHTUS," *European Conference For Aerospace Sciences (EUCASS)*, Brussels, July 2007; also *Advances in Aerospace Sciences*, Vol. 1, European Conference For Aerospace Sciences Book Series, edited by L. DeLuca, C. Bonnal, O. Haidn, and S. Frolov (to be published).

[9] Liepmann, H. W., and Roshko, A., *Elements of Gasdynamics*, 3rd ed., Wiley, New York, 1960.

[10] Vermeulen, P. J., Boddie, W. L., and Wierum, F. A., "State Control of a Flowing Plasma by Means of Radio Frequency Electromagnetic Fields," *AIAA Journal*, Vol. 5, No. 5, 1967, pp. 1015–1017. doi:10.2514/3.4116

[11] Poole, J., and Vogel, C., "Induction Plasma Nozzle Tests," NASA CR-1765, April 1971.

[12] Yoshida, T., Toshihiko, T., Nishimura, H., and Akashi, K., "Characterization of a Hybrid Plasma and its Application to Chemical Synthesis," *Journal of Applied Physics*, Vol. 54, No. 2, 1983, pp. 640–646. doi:10.1063/1.332070

[13] Seo, J. H., Hwang, J. S., Nam, S. J., Choi, S. I., and Hong, S. H., "Enthalpy Probe Analysis on Thermal Plasma Characteristics of DC-RF Hybrid Plasma Jets," *16th International Symposium on Plasma Chemistry*, Taormina, Italy, June 2003.

[14] Seo, J. H., Nam, J. S., Hwang, J. S., Lee, C. M., Choi, S. I., and Hong, S. H., "Water- Cooled Electrostatic Probe Measurements on the Temperature of Electron and Heavy Particle in DC–RF Hybrid Plasma Jets," *30th International Conference on Plasma Science (ICOPS)*, Jeju, Korea, June 2003.

[15] "Electromagnetic Intelligent Fluids Laboratory," Institute of Fluid Science, Tohoku Univ., Japan, http://www.ifs.tohoku.ac.jp/nishiyama-lab/.

[16] Leon, H., and Mickelsen, W., "Theoretical Analyses of Electrothermal Thruster with Supersonic Heat Addition," *Journal of Spacecraft and Rockets*, Vol. 6, No. 12, 1969, pp. 1362–1366. doi:10.2514/3.29831

[17] Chavers, G., Chang–Diaz, F., Irvine, C., and Squire, J., "Momentum and Heat Flux Measurements Using an Impact Target in Flowing Plasma," *Journal of Propulsion and Power*, Vol. 22, No. 3, 2006, pp. 637–644. doi:10.2514/1.1971

[18] Eckert, H. U., "The Induction Arc: A State-of-the-Art Review," *High Temperature Science*, Vol. 6, 1974, pp. 99–134.

[19] Herdrich, G., Auweter–Kurtz, M., Kurtz, H., Laux, T., and Winter, M., "Operational Behavior of Inductively Heated Plasma Source IPG3 for Entry Simulations," *Journal of Thermophysics and Heat Transfer*, Vol. 16, No. 3, 2002, pp. 440–449. doi:10.2514/2.6698

[20] Wichmann, H. G., "Über die Bestimmung des Schubs von Elektrodenlosen Magnetohydrodynamischen Triebwerken," *Jahrbuch 1963 der Wissentschaftlichen Gesellschaft für Luft- und Raumfahrt*, edited by H. Blenk, Viewig, Brunswick, Germany, 1964, pp. 382–388.

[21] Gölz, T., Auweter–Kurtz, M., and Kurtz, H., "Development and Testing of a 100 kW Radiation Cooled Thermal Hydrogen Arcjet Thruster," International Electric Propulsion Conference, Paper IEPC-1993-221, Seattle, WA, Sept. 1993.

[22] Kurtz, H., Auweter–Kurtz, M., Glocker, B., Merke, W., and Schrade, H. O., "A 15 kW Experimental Arcjet," International Electric Propulsion Conference, Paper IEPC-88-107, Garmisch–Partenkirchen, Germany, Sept. 1988.

[23] Frohn, A., *Einführung in die Technische Thermodynamik*, 2nd ed., Springer–Verlag, Berlin, 1989.

[24] Laure, S., "Experimentelle Simulation der Staupunktströmung Wiedereintretender Raumflugkörper und Deren Charakterisierung Mittels Mechanischer Sonden," Ph.D. Dissertation, Universität Stuttgart, 1998.

[25] Laure, S., Auweter–Kurtz, M., Fasoulas, S., Habiger, H., and Schönemann, A., "Experimentelle Simulation einer Hochenthalpen Luftströmung im Plasmawindkanal," *Jahrbuch der Deutschen Gesellschaft für Luft- und Raumfahrt*, Vol. 3, DGLR, Erlangen, Germany, 1994.

[26] Abramovich, G. N., *Theory of Turbulent Jets*, MIT Press, Cambridge, MA, 1963, p. 269.

[27] Hiers, R., and Pruitt, D., "Determination of Thrust from Pitot Pressure Measurements," AIAA Paper 2001-3314, July 2001.

[28] Anderson, J. D., *Hypersonic and High Temperature Gas Dynamics*, Series in Aeronautical and Aerospace Engineering, McGraw–Hill New York, 1989.

[29] Vincenti, W. G., and Kruger, C. H., *Introduction to Physical Gas Dynamics*, Wiley, New York, 1965.

[30] Fasoulas, S., Sleziona, C., Auweter–Kurtz, M., Habiger, H., Laure, H., and Schönemann, A., "Characterization of a Nitrogen Flow Within a Plasma Wind Tunnel," *Journal of Thermophysics and Heat Transfer*, Vol. 9, No. 3, 1995, pp. 422–431. doi:10.2514/3.684

E. Choueiri
Associate Editor